Circulation

ORIGINAL RESEARCH ARTICLE

TBX5 and CHD4 Coordinately Activate Atrial Cardiomyocyte Genes to Maintain Cardiac Rhythm Homeostasis

Mason E. Sweat, PhD*; Wei Shi, PhD*; Yan Y. Sweat, PhD; Jie Li, MD; Jiajin Li, MD; Erin M. Keating, BS; Anna Ponek, BS; Qing Ma, MD; Chaehyoung Park, BS; Michael A. Trembley, PhD; Yi Wang, PhD; Cuilan Hou, PhD; Vassilios J. Bezzerides, MD, PhD; Frank L. Conlon, PhD; William T. Pu, MD

BACKGROUND: Atrial fibrillation, the most common sustained arrhythmia, affects 59 million individuals worldwide. The transcription factor TBX5 (T-box 5) is essential for normal atrial rhythm. Its inactivation causes loss of atrial cardiomyocyte (aCM) enhancer accessibility, looping, transcriptional identity, and spontaneous atrial fibrillation. TBX5 interacts with CHD4 (chromodomain helicase DNA-binding protein 4), a chromatin remodeling ATPase canonically associated with the NuRD (nucleosome remodeling and deacetylase) repressor complex.

METHODS: We investigated mechanisms by which TBX5 regulates chromatin organization by studying mice with aCM-selective inactivation of TBX5 or CHD4. We integrated multiple genomics approaches including concurrent single-nucleus transcriptome and open chromatin profiling and genome-wide TBX5 and CHD4 chromatin occupancy assays.

RESULTS: We found that TBX5 recruits CHD4 to 33 170 genomic regions (TBX5-enhanced CHD4 sites). In addition to the canonical repressive activity of CHD4, we uncovered a CHD4 activator function predominantly at sites to which it was recruited by TBX5. TBX5-enhanced CHD4 recruitment increased local chromatin accessibility and promoted the expression of aCM identity genes. This mechanism of CHD4 recruitment by TBX5 was crucial for sinus rhythm; mice with CHD4 inactivation in aCMs had increased atrial fibrillation vulnerability. Assaying TBX5 binding in *Chd4*^{AKO} atria demonstrated that CHD4 also promotes TBX5 binding at >10 000 genomic loci, including 3051 TBX5-enhanced CHD4 sites. Consistent with its requirement to maintain normal atrial rhythm, CHD4 was implicated in the regulation of 42 genes linked to atrial fibrillation in humans. Nine had the hallmarks of TBX5-dependent, CHD4-mediated transcriptional activation.

CONCLUSIONS: Our findings reveal that normal atrial rhythm requires CHD4, which activates and represses atrial genes in a context-dependent manner to maintain aCM gene expression, aCM identity, and atrial rhythm homeostasis.

Key Words: arrhythmias, cardiac ■ atrial fibrillation ■ transcription factors

Atrial cardiomyocytes (aCMs) and ventricular cardiomyocytes (vCMs) are highly specialized to achieve their distinct roles in the cardiac cycle. These specialized features are maintained and coordinated by the differential expression of thousands of genes.[1,2] Chamber selective gene expression is, in turn, regulated by aCM- or vCM-specific epigenetic regulatory programs and aCM- or vCM-specific chromatin organization.[1,3] Abnormalities of aCM function can lead to atrial fibrillation (AF), the most common sustained human arrhythmia,[4] when atrial impulse conduction becomes disorganized and forms fractionated, self-sustaining wavelets, causing uncoordinated atrial contraction and rapid and irregularly irregular activation of the ventricles.[5]

Correspondence to: William T. Pu, MD, Department of Cardiology, Boston Children's Hospital, 300 Longwood Ave, Boston, MA 02115, Email william.pu@cardio.chboston.org; or Frank L. Conlon, PhD, Department of Biology, University of North Carolina at Chapel Hill, Chapel Hill, NC 27599, Email frank_conlon@med.unc.edu
This manuscript was sent to Ju Chen, PhD, Guest Editor, for review by expert referees, editorial decision, and final disposition.
*M.E. Sweat and W. Shi contributed equally.
Supplemental Material is available at https://www.ahajournals.org/doi/suppl/10.1161/CIRCULATIONAHA.125.073833.
For Sources of Funding and Disclosures, see page 799.

Circulation is available at www.ahajournals.org/journal/circ

Clinical Perspective

What Is New?

- TBX5 (T-box 5), a transcription factor implicated in human atrial fibrillation (AF) by genome-wide association studies, regulates atrial cardiomyocyte gene transcription by recruiting a chromatin remodeling enzyme, CHD4 (chromodomain helicase DNA binding protein 4), to control the accessibility of cis-regulatory elements.
- Preventing this mechanism through *Chd4* deletion in atrial cardiomyocytes resulted in partially penetrant spontaneous AF and increased AF vulnerability in mice.
- In addition to its established role as a transcriptional repressor, we identified a novel activity of CHD4 as a transcriptional activator in atrial cardiomyocytes, which promotes the binding of TBX5.

What Are the Clinical Implications?

- CHD4 is a new component of the atrial gene regulatory network, which becomes dysregulated in AF.
- As an epigenetic remodeling enzyme, CHD4 may contribute to epigenetic memory, which is likely central to the inexorable progression of paroxysmal to permanent AF.

Nonstandard Abbreviations and Acronyms

AAV9	adeno-associated virus serotype 9
aCM	atrial cardiomyocyte
AF	atrial fibrillation
AKO	atrial knockout
BAF	Brg1/Brm-associated factor
BRG1	brahma-related gene 1
***Brg1*^{AKO}**	*Brg1* inactivation in postnatal atrial cardiomyocytes
CHD4	chromodomain helicase DNA binding protein 4
***Chd4*^{AKO}**	atrial-selective *Chd4* knockout
ChIP-seq	chromatin immunoprecipitation followed by next-generation sequencing
CTCF	CCCTC-binding factor
CUT&RUN	cleavage under targets and release using nuclease
DAR	differentially accessible region
DEG	differentially expressed gene
GTEX	Genotype-Tissue Expression Project
H3K27ac	histone H3 acetylated on lysine 27
MEF2	myocyte enhancer factor 2
NuRD	nucleosome remodeling and deacetylase
PCM1	pericentriolar material 1
RNA-seq	RNA sequencing
SDRR	SD of the RR interval
snATAC-seq	single-nucleus assay for transposase-accessible chromatin using sequencing
snRNA-seq	single-nucleus RNA sequencing
SRF	serum response factor
TBX5	T-box 5
***Tbx5*^{AKO}**	atrial-selective *Tbx5* knockout
TEAD1	TEA domain family member 1
TF	transcription factor
vCM	ventricular cardiomyocyte
WT	wild-type

AF elevates the risk of stroke and heart failure and increases health care costs in the United States by >$28 billion each year.[5]

The transcription factor (TF) TBX5 (T-box 5) is essential for postnatal aCM identity.[6–8] TBX5 inactivation caused loss of chromatin accessibility, the active enhancer mark H3K27ac, and promoter contacts of aCM enhancers.[9] TBX5 aCM inactivation caused the loss of atrial identity and spontaneous AF.[9–11] The ability of TBX5 to maintain enhancer accessibility is likely facilitated by interactions with chromatin remodeling proteins. TBX5 interacts genetically and physically with 2 different chromatin remodelers. The BAF complex (Brg1/Brm-associated factor) facilitates the expression of direct TBX5 target genes *NPPA* and *BMP10*, and BRG1 (brahma-related gene 1) and TBX5 physically and genetically interact to promote normal heart development.[12,13] TBX5 also physically interacts with CHD4 (chromodomain helicase DNA binding protein 4), the core nucleosome-remodeling enzyme of the repressive NuRD (nucleosome remodeling and deacetylase) complex.[14] *Chd4* deletion in developing and postnatal cardiomyocytes resulted in the upregulation of sarcomeric proteins from noncardiomyocyte muscle lineages, including Acta1 from skeletal muscle and Myh11 from smooth muscle.[15,16]

In this study, we show that atrial-selective *Chd4* knockout (*Chd4*^{AKO}) increased AF vulnerability and caused partially penetrant spontaneous AF. TBX5 recruitment of CHD4 both activated and repressed genes in aCMs. Consistent with previous studies,[15,16] TBX5 recruited CHD4 to repress noncardiomyocyte lineage genes. In addition, we reveal an unappreciated gene-activating function of CHD4, in which TBX5-recruited CHD4 activated aCM genes. Our findings demonstrate that CHD4-mediated gene activation and repression are crucial to aCM gene regulation and atrial rhythm homeostasis.

METHODS

Detailed Methods and a Major Resources Table are provided in the Supplemental Material. Animal research was conducted under protocols approved by the Institutional Animal Care and Use Committees at Boston Children's Hospital or the University of North Carolina, Chapel Hill.

Statistics

Statistical tests were performed in PRISM or R with P=0.05 as the significance threshold.

Data Availability

New sequencing data generated by the study were deposited in Gene Expression Omnibus with accession numbers GSE284093 (Multiome), GSE284094 (bulk RNA sequencing [RNA-seq]), GSE284095 (chromatin immunoprecipitation followed by next-generation sequencing [ChIP-seq]), and GSE296675 (cleavage under targets and release using nuclease [CUT&RUN]). All other data supporting the findings in this study are included in the main article and associated files. Resources used in the study are available upon request.

RESULTS

BRG1 Inactivation Does Not Alter TBX5 Target Gene Expression

TBX5 deletion caused loss of accessibility at enhancer elements promoting aCM-selective gene expression (Figure 1A). To determine whether TBX5 activity depends on BRG1, a TBX5 coactivator,[13] we injected postnatal day 3 *Brg1*$^{flox/flox}$ pups[17] with adeno-associated virus serotype 9 (AAV9) with the aCM-selective *Nppa* promoter driving *Cre* (AAV9:*Nppa-Cre*)[9,18] or AAV9:*Nppa-EGFP* as a negative control. *Brg1* inactivation in postnatal aCMs (*Brg1*^{AKO}) did not significantly affect expression of previously validated TBX5 targets *Tbx5*, *Nppa*, *Nppb*, *Myl7*, *Scn5a*, *Atp2a2*, or *Ryr2* (Figure S1A).[9,11] Mice with aCM-selective inactivation of *Tbx5* (*Tbx5*^{AKO}) developed spontaneous AF by postnatal day 21.[9] ECGs at postnatal day 28 showed that *Brg1*^{AKO} mice remained in normal sinus rhythm (Figure S1B and S1C). We concluded that the *Tbx5*-regulated postnatal aCM gene regulatory network is not dependent on *Brg1*.

TBX5 Enhances CHD4 Chromatin Occupancy in aCMs

We turned our attention to CHD4, another chromatin remodeler that interacts with TBX5.[14] To determine whether TBX5 actively recruits CHD4 in aCMs, we measured CHD4 occupancy in *Tbx5*^{AKO} and control aCMs (Figure 1B). Neonatal *Tbx5*$^{flox/flox}$ mice were treated at postnatal day 3 with either AAV9:*Nppa-Cre* or AAV9:*Nppa-EGFP*. Nuclei marked by PCM1 (pericentriolar material 1), selectively expressed on cardiomyocyte nuclei, were isolated from 3-week-old atria in biological duplicate. We used ChIP-seq to measure CHD4 chromatin occupancy. Diffbind[19] differential occupancy analysis identified 33 170 genomic loci enriched in control samples compared with *Tbx5*^{AKO} samples (Tbx5-enhanced regions; Figure 1C and Table S1). Of these, 12 134 (36.6%) regions were occupied by TBX5 in aCMs, based on our previously reported data.[1] Far fewer CHD4 regions had greater Chd4 binding in *Tbx5*^{AKO} samples (363 Tbx5-impaired CHD4 regions). A total of 60 810 (64.5%) CHD4 regions were not significantly enriched in either sample type, consistent with recruitment of CHD4 by other TFs.[20]

To identify regulators of the TBX5-enhanced CHD4 regions, we performed motif enrichment analysis. In addition to the TBX5 motif, we detected enrichment for the MEF2 (myocyte enhancer factor 2) and GATA4 motifs (Figure 1D): cardiac TFs that interact with[21–23] and frequently co-occupy regions with TBX5.[1,24,25] TBX5-enhanced CHD4 regions were also enriched for the motif of CTCF (CCCTC-binding factor), a TF that interacted with CHD4 in cardiomyocytes by CHD4 immunoprecipitation and mass spectrometry.[26]

TBX5-enhanced CHD4 binding regions were disproportionately located within gene promoters (±1 kb of the transcription start site [0.7%]; Figure 1E). Other common locations included introns (38.5%) and distal intergenic regions (23.14%). TBX5-impaired regions were also enriched at promoter regions (12.4%), but to a lesser degree than TBX5-enhanced regions (Figure 1F).

Together, these data indicate that TBX5 enhances CHD4 chromatin occupancy at regions co-occupied by TBX5.

CHD4 Inactivation Causes Atrial Remodeling and Immune Cell Infiltration

To identify effects of CHD4 inactivation in postnatal aCMs, we injected AAV9:*Nppa-Cre* or AAV9:*Nppa-EGFP* (control) into postnatal day 3 *Chd4*$^{flox/flox}$ pups (Figure 2A). Echocardiography revealed that left ventricular size and function were comparable between AAV9:*Nppa-Cre* (*Chd4*^{AKO}) and control mice at 1 to 3 months (Figure 2B). Heart sections from 2- to 3-month-old mice confirmed efficient and selective loss of CHD4 in *Chd4*^{AKO} aCMs (Figure 2C) but not vCMs (Figure 2D).

Fibrotic remodeling is a hallmark of atrial dysfunction. We assessed fibrosis with picrosirius red/fast green staining on 2- to 3-month-old control and *Chd4*^{AKO} heart sections (Figure 2E and 2F). *Chd4*^{AKO} mice had greater atrial fibrosis, whereas there was no difference in ventricular fibrosis. Staining for the panimmune cell marker CD45 demonstrated greater numbers of immune cells in *Chd4*^{AKO} atria compared with controls (Figure 2G), consistent with observations in human and mouse models of AF.[27]

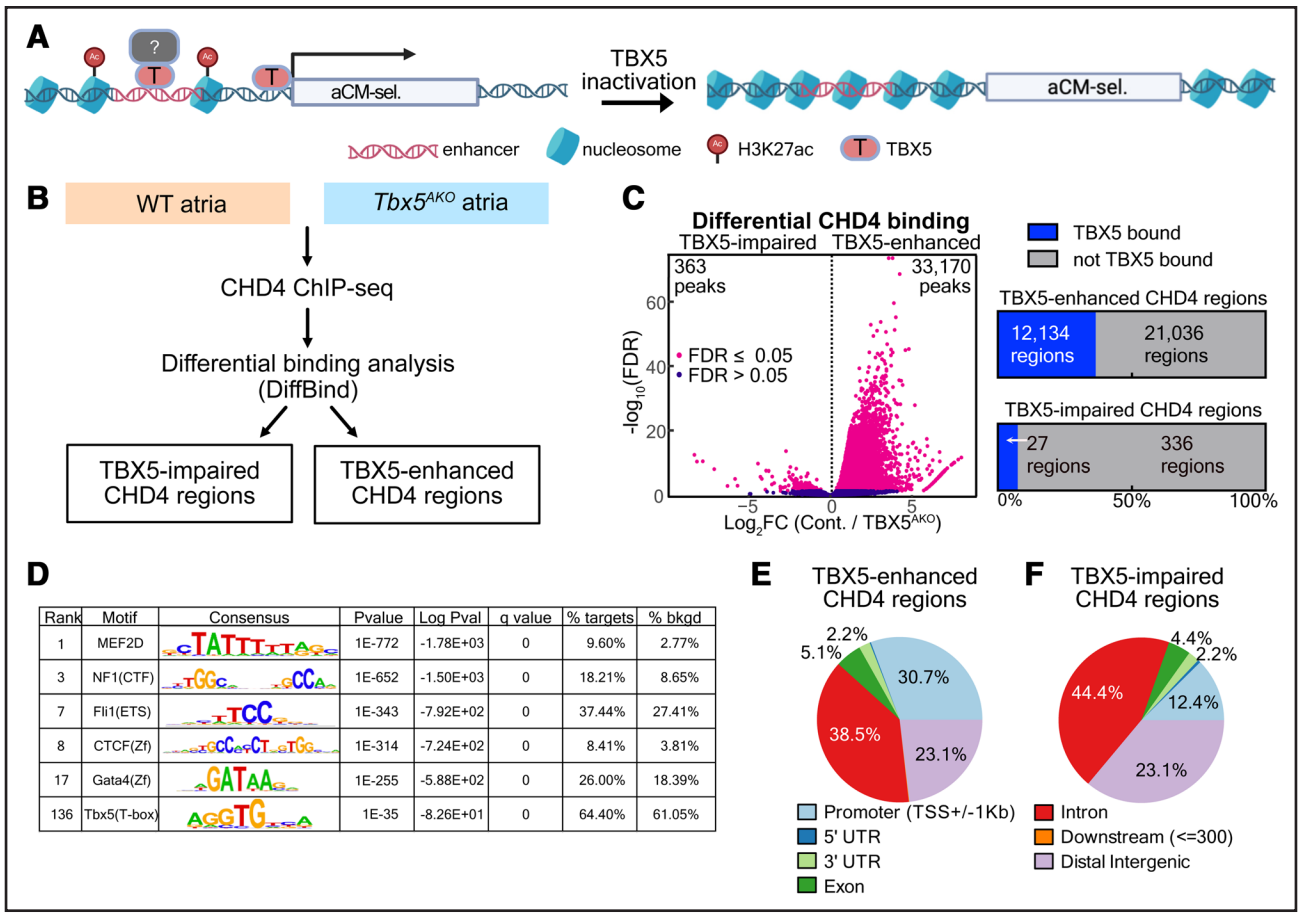

Rank	Motif	Consensus	Pvalue	Log Pval	q value	% targets	% bkgd
1	MEF2D		1E-772	-1.78E+03	0	9.60%	2.77%
3	NF1(CTF)		1E-652	-1.50E+03	0	18.21%	8.65%
7	Fli1(ETS)		1E-343	-7.92E+02	0	37.44%	27.41%
8	CTCF(Zf)		1E-314	-7.24E+02	0	8.41%	3.81%
17	Gata4(Zf)		1E-255	-5.88E+02	0	26.00%	18.39%
136	Tbx5(T-box)		1E-35	-8.26E+01	0	64.40%	61.05%

Figure 1. TBX5 recruits CHD4 to genomic loci.
A, Model of *TBX5* gene regulation in atrial cardiomyocytes (aCMs). *TBX5* inactivation results in the loss of enhancer accessibility and downregulation of aCM-selective genes. **B**, CHD4 chromatin immunoprecipitation followed by next-generation sequencing (ChIP-seq) experimental design. Five animals were used per biological replicate, and 2 replicates were performed per group. **C**, Diffbind analysis of CHD4 (chromodomain helicase DNA binding protein 4) binding in control and *Tbx5*^{AKO} samples. Significant regions ($|Log_2FC|>0.5$, false discovery rate [FDR]<0.05) are colored red. On the right, the intersection of statistically significant regions with TBX5 (T-box 5) occupancy data obtained from TBX5 bioChIP-seq in postnatal aCMs (GSE215065). **D**, Motif enrichment analysis of TBX5-enhanced CHD4 regions. q value, hypergeometric test with BH correction. **E** and **F**, Location of TBX5-enhanced and TBX5-impaired CHD4 regions with respect to genome annotations. WT indicates wild-type.

CHD4 Inactivation Increases Atrial Fibrillation Vulnerability

Because *Tbx5*^{AKO} mice rapidly develop spontaneous AF[9] with 100% penetrance, we investigated the rhythm of *Chd4*^{AKO} mice. We recorded surface ECGs and scored rhythm regularity using the SD of the RR interval (SDRR; Figure 3A). Before 3 months of age, SDRR was comparable between groups, suggesting that most mice remained in a regular rhythm. At 4 to 5 months old, there was a tendency toward elevated SDRR (*P*=0.051). Analysis of the beat-to-beat variation in RR interval indicated irregularly irregular rhythm in *Chd4*^{AKO} mice with high SDRR, consistent with spontaneous AF (Figure 3B). Out of 15 mice studied, one 5-week-old mouse and three 5-month-old mice had markedly elevated SDRR, irregularly irregular rhythm, and no P waves—hallmarks of AF—compared with 0 of 12 in the control group (Figure 3C).

We tested the AF vulnerability of *Chd4*^{AKO} mice at 23 months of age by right atrial pacing (Figure 3D). A greater proportion of *Chd4*^{AKO} mice were induced to develop sustained AF (lasting >3 seconds; Fisher exact test *P*=0.0075) compared with controls (Figure 3E). The duration of induced AF was also increased in *Chd4*^{AKO} mice, including in 3 mice that did not recover normal rhythm by 5 minutes, the study end point (Figure 3F).

These data indicate that loss of CHD4 in aCMs increases AF vulnerability.

CHD4 and TBX5 Coordinately Regulate Atrial Gene Expression

TBX5 recruitment of CHD4 to genomic loci suggested that these proteins cooperatively regulate gene expression in postnatal aCMs.[15,20] To test this hypothesis, we

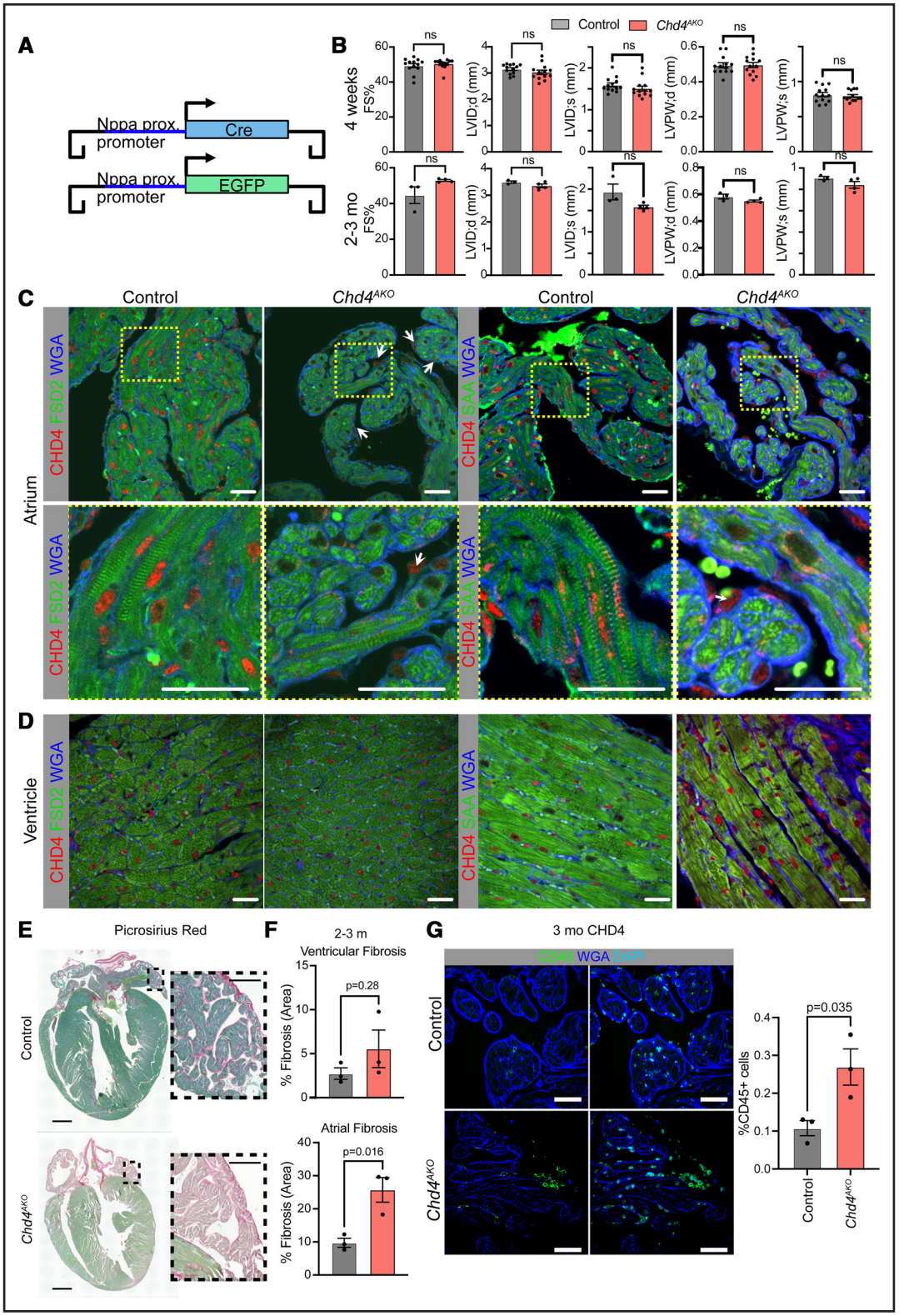

Figure 2. Inactivation of CHD4 in atrial cardiomyocytes results in atrial remodeling.
A, Schematic of the adeno-associated virus serotype 9 (AAV9):*Nppa-EGFP* and AAV9:*Nppa-Cre* AAV constructs. *Chd4*$^{flox/flox}$ mice that received AAV9:*Nppa-EGFP* and AAV9:*Nppa-Cre* were designated control and *Chd4*^{AKO}, respectively. **B**, Echocardiographic assessment of left ventricular size and function. Studies were performed at 4 weeks and 2 to 3 months after AAV injection (4 weeks, n=13 per group; 2–3 months, n=3 control and 4 *Chd4*^{AKO}; 2-tailed *t* test, NS, *P*>0.05). **C** and **D**, Confocal images of immunostained atrial and ventricular sections. White arrows in the *Chd4*^{AKO} images denote cells that retained CHD4 (chromodomain helicase DNA binding protein 4) expression. Yellow boxed areas are enlarged in the second row of panels. Scale bars=20 μm. **E**, Picrosirius red staining of control and *Chd4*^{AKO} heart (*Continued*)

Figure 2 Continued. sections (scale bars=1 mm). Boxed areas are enlarged to the right (scale bars, 250 µm). Images are representative of 3 independent experiments. **F**, Quantification of fibrotic area (n=3 mice per group; unpaired *t* test). **G**, Confocal images of immunostained atrial sections from 3-month-old mice. Scale bar=40 µm. Right, quantification of the percentage of CD45+ cells per section compared with the total number of cells (n=3 mice per group; unpaired *t* test). LVIDd indicates left ventricular internal dimension at end-diastole; LVIDs, left ventricular internal dimension at end-systole; LVPWd, left ventricular posterior wall thickness at end-diastole; and LVPWs, left ventricular posterior wall thickness at end-systole.

performed bulk RNA-seq of postnatal day 21 *Chd4*^{AKO} and control atria (n=4/group; Figure 4A). Principal component analysis demonstrated a clear separation of the *Chd4*^{AKO} and control samples along principal component 1 (Figure 4B). We identified 2748 differentially expressed genes (DEGs; $|Log_2FC|>0.5$ and $P_{adjusted}<0.05$): 1077 with greater expression in controls and 1671 with greater expression in *Chd4*^{AKO} (Table S2 and Figure 4C).

To determine whether CHD4 regulated TBX5 target genes, we examined a curated list of aCM-selective genes that are downregulated (*Sbk2*, *Sbk3*, *Myl7*, *Nppa*, *Myl4*, and *Fgf12*) or upregulated (*Lrrc4*, *Fbn2*, *Kcnq5*, *Casq1*, and *Nrg1*) in *Tbx5*^{AKO} aCMs[9] (Figure 4D). For these selected targets, gene expression changes between wild-type (WT) and *Chd4*^{AKO} atria were largely comparable to differences between WT and *Tbx5*^{AKO} aCMs. Gene Ontology term analysis revealed that genes more highly expressed in control samples were related to muscle function (Figure 4E). Genes upregulated in *Chd4*^{AKO} samples were related to lymphocyte activation and atrial remodeling (Figure 4F), consistent with the atrial remodeling, fibrosis, and immune cell infiltration that we observed in *Chd4*^{AKO} atria (Figure 2E–2G).

We compared the quantitative change in gene expression in the *Chd4*^{AKO} bulk RNA-seq and our previously reported TBX5 aCM knockout (*Tbx5*^{AKO}) single-nucleus RNA-seq (snRNA-seq) assays[9] (Figure S2A). Most genes differentially expressed in both experiments were altered in the same direction by TBX5 or CHD4 inactivation (purple points in quadrants I and III). In each data set, genes with aCM-selective expression were more highly expressed in WT compared with the AKO group (Figure S2B), consistent with CHD4 and TBX5 promoting their expression. In total, CHD4 and TBX5 coordinately promoted and repressed the expression of 513 and 633 genes, respectively (Figure S2C and S2D). This overlap between CHD4 and TBX5 DEGs was highly significant (hypergeometric test: $P<2.5E{-}34$). Genes activated by both factors facilitate metabolism and nucleotide biosynthesis, whereas genes repressed by both CHD4 and TBX5 were related to extracellular matrix remodeling and transforming growth factor β signaling (Figure S2E). Gene Ontology analysis of genes upregulated in *Chd4*^{AKO} and downregulated in *Tbx5*^{AKO} (Figure S2E; Quadrant IV) revealed terms associated with ion transport and cardiac muscle contraction, perhaps explaining the lower incidence of spontaneous AF observed in *Chd4*^{AKO} mice compared with *Tbx5*^{AKO} mice.

Multiomic Analysis of Control and *Chd4*^{AKO} Mouse Atria

Given CHD4's role in chromatin remodeling, we performed concurrent snRNA-seq and snATAC-seq (single-nucleus assay for transposase-accessible chromatin using sequencing) on *Chd4*^{AKO} and control atria. In total, 4 *Chd4*^{AKO} samples and 2 control samples were processed, with each sample consisting of a right and left atrium from 2 mice (1 male and 1 female; Table S3). For the *Chd4*^{AKO} samples, 7 of the 8 mice had inducible (4; 3.5 months old) or spontaneous (3; 5 months old) AF. Control samples were from 5-month-old WT mice. After doublet removal and rigorous quality control (see Methods), we obtained 27 263 high-quality nuclei (Figure S3A and S3B). The snRNA and snATAC data were integrated using a weighted nearest neighbors approach, grouped by Louvain clustering, and visualized using uniform manifold and approximation projection (Figure S3C). Data were highly concordant between genotypes and we observed minimal batch effect between samples (Figure S3D and S3E).

Cell states were annotated using atrial cell marker genes (Figure S4A). We removed a small cluster of likely residual doublets with high expression of epicardial and immune cell markers. A small cluster of vCMs was identified in control samples (Figure S4A and S4B). aCM_1, the largest aCM cluster, contained predominantly control nuclei, as did the smaller aCM clusters aCM_3 and aCM_4 (Figure S4C). In contrast, the second largest aCM cluster, aCM_2, derived nearly exclusively from *Chd4*^{AKO} samples (magenta dotted line, Figure S3D and Figure S4B). There was also genotype-specific enrichment for endocardial (endocardium_3, control; endocardium_2, *Chd4*^{AKO}) and macrophage (macrophage_3, control; macrophage_2, *Chd4*^{AKO}) clusters.

CHD4 Controls the aCM Identity Gene Program

To determine whether aCM_2 represented *Chd4*^{AKO} aCMs, we projected *Cre* expression onto the weighted nearest neighbor uniform manifold and approximation projection (Figure 5A and 5B). *Cre* expression was largely confined to aCM_2, identifying them as *Chd4*^{AKO} aCMs. We identified DEGs between aCM_2 and aCM_1, the largest control aCM cluster (Figure 5A and 5B). A total of 2256 DEGs ($|Log_2FC|>0.5$ and $P_{adjusted}<0.05$) were identified, with 431 and 1825 higher aCM_1 and

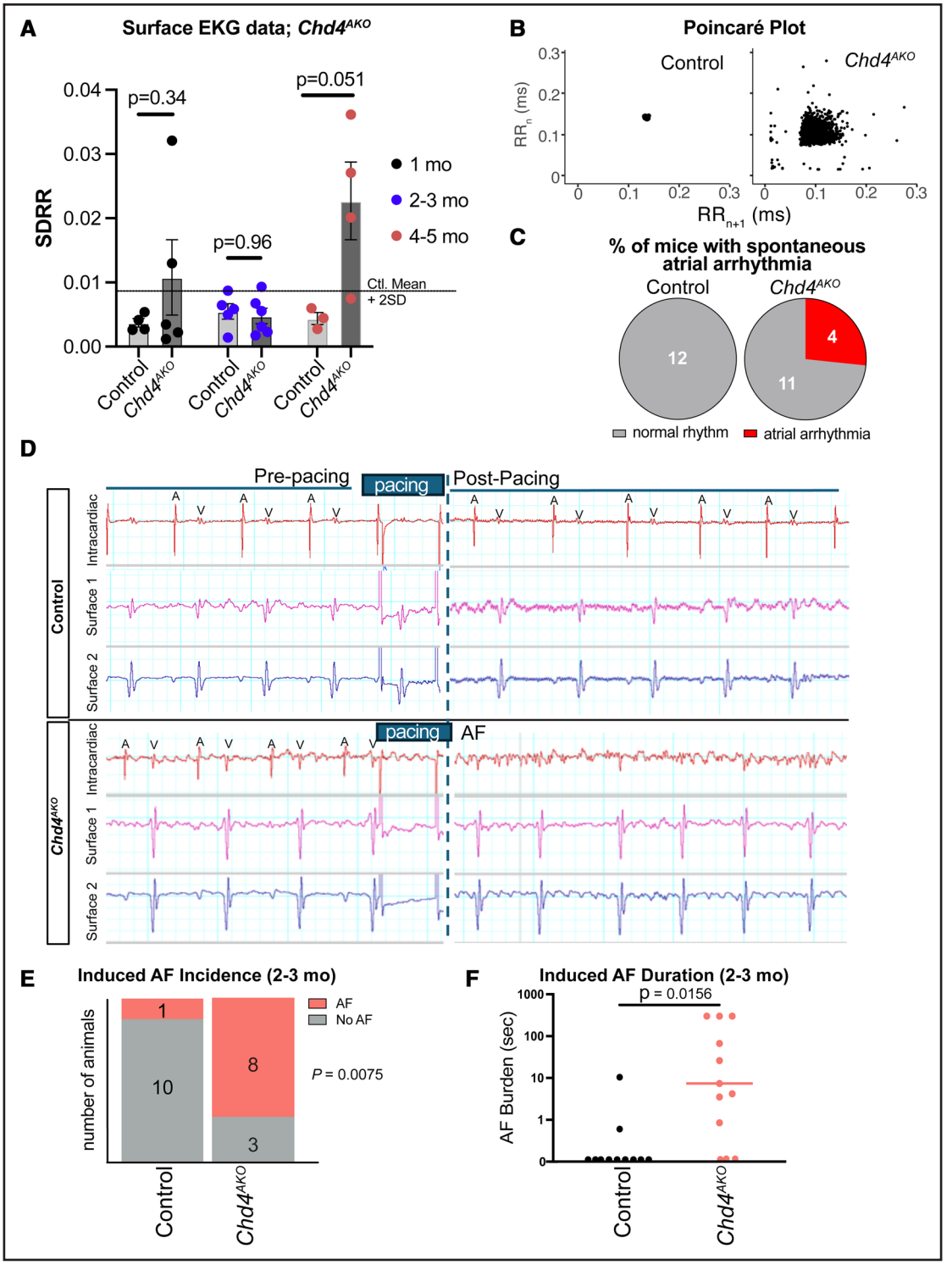

Figure 3. CHD4 inactivation in atrial cardiomyocytes increases atrial fibrillation vulnerability.
A, Irregularity of cardiac rhythm was assessed from surface ECGs using SD of the RR interval (SDRR). SDRR was not significantly elevated at any time point, but 4 mice (1 at 4–5 weeks and 3 at 4–5 months) had elevated SDRR. Surface ECGs of these mice showed a loss of P waves, consistent with atrial fibrillation (AF). Unpaired *t* test. The dotted line represents the upper limit of normal for control mice (mean+2 SD; 1 month, n=4 controls and 5 *Chd4*^{AKO}; 3 months, n=5 controls and 6 *Chd4*^{AKO}; 4–5 months, n=3 controls and 4 *Chd4*^{AKO}). **B**, Representative Poincaré plot of a control mouse and a *Chd4*^{AKO} mouse with high SDRR, showing the beat-to-beat variation in RR interval. **C**, Proportion of mice with spontaneous atrial arrhythmias. **D**, Representative data from programmed atrial stimulation experiments. The atrial rhythm was recorded by an intracardiac electrode, and the surface ECG was captured by limb leads. After the pacing protocol, the atrial recording was evaluated for AF. **E**, AF incidence after programmed atrial simulation of 2- to 3-month-old mice. One of 11 controls and 8 of 11 *Chd4*^{AKO} mice had AF for >3 seconds after pacing. Fisher exact test. **F**, AF burden of the 2- to 3-month-old cohort of paced mice. AF burden is the total duration of AF after atrial pacing. Wilcoxon test. A indicates atrial signal; and V, ventricular signal.

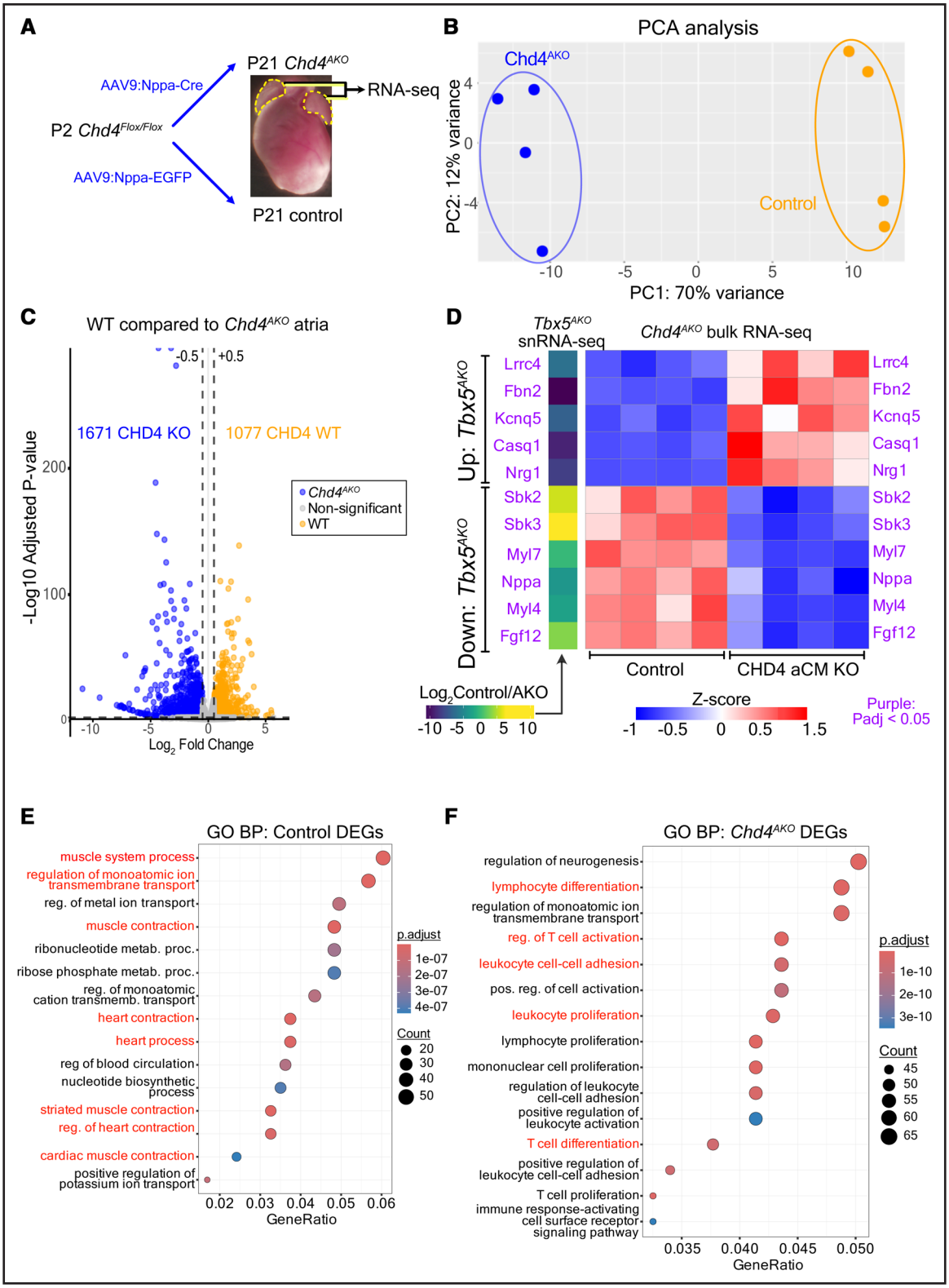

Figure 4. Bulk RNA sequencing of postnatal day 21 control and Chd4AKO atria.
A, Experimental design. Postnatal day 21 (P21) right and left atria from 4 control mice and 4 *Chd4*^{AKO} mice were used in the experiment. **B**, Principal component analysis (PCA) of wild-type (WT) and *Chd4*^{AKO} RNA sequencing samples. **C**, Differentially expressed genes (DEGs) between WT and *Chd4*^{AKO} atria. Significant DEGs, $|Log_2FC|>0.5$ and $P_{adjusted}<0.05$. *P* values, Wald test with Benjamini-Hochberg (BH) correction. **D**, Heatmap of atrial cardiomyocyte (aCM)–selective TBX5 (T-box 5) target genes and genes upregulated in TBX5 knockout (KO) aCMs in single-nucleus RNA sequencing data from WT and *Tbx5*^{AKO} aCMs compared with WT and *Chd4*^{AKO} atria. Gene symbols in purple were significantly differentially expressed in control vs KO samples in both *Tbx5* and *Chd4* KO experiments. *P* values for TBX5 single-cell experiment, (*Continued*)

Figure 4 Continued. Wilcoxon test with BH correction. **E** and **F**, Gene Ontology (GO) enrichment terms enriched for control or *Chd4*^{AKO} DEGs. The *x* axis shows the ratio of the number of genes in the intersection of DEGs and the gene set to the total genes in the gene set. Data points are colored by the adjusted *P* value, and data point size corresponds to the total number of genes for each term. GO terms highlighted in red are of particular biological interest. Adjusted *P* values, hypergeometric test with BH adjustment.

aCM_2, respectively (Table S4). DEGs from this snRNA-seq comparison agreed with those from the bulk RNA-seq of control and *Chd4*^{AKO} atria (Pearson r=0.835; *P*=1.9E−302; Figure S5A), as did Gene Ontology terms enriched for DEGs more highly expressed in control or *Chd4*^{AKO} aCMs (Figure 5D). *Chd4*^{AKO} DEGs were related to chamber remodeling, whereas control DEGs were related to muscle function, cell junction assembly, and cardiac rhythm.

To determine whether CHD4 regulates aCM identity, aCM- and vCM-selective genes were overlaid with DEGs from the aCM_2 vs aCM_1 comparison (Figure 5E). aCM-selective genes were overrepresented among genes activated versus repressed downstream of *Chd4* (26% [112 of 413] versus 12% [213 of 1825]; Fisher exact test *P*=9.1E−13). In contrast, we did not observe significant enrichment of vCM-selective genes among genes activated or repressed downstream of *Chd4*.

In fetal and postnatal cardiomyocytes, CHD4 binds cardiac TFs, including TBX5, to repress the expression of skeletal and smooth muscle genes.[15,16] To determine whether this function is conserved in aCMs, we examined the top ≈100 DEGs ranked by significance in aCM_1 and aCM_2 for their expression levels in human left ventricle, atrial appendage, skeletal muscle, and coronary arteries, and their hallmark muscle cells from the Genotype-Tissue Expression Project, a bulk and snRNA-seq atlas of human gene expression (Figure S5B and S5C). Top-ranked DEGs activated by CHD4 were highly expressed in atrial appendage and ventricle, with few showing enrichment in coronary artery or skeletal muscle, or their related myocyte subtypes. In contrast, top-ranked DEGs repressed by CHD4 were enriched in skeletal muscle tissue and myocytes (eg, *Myl3*, *Tnnt3*, *Tnnt1*, *Tnni1*, *Atp2a1*, *Acta1*, *Casq1*, *Ypl2*, *Scn1b*) or in coronary artery tissue and smooth muscle myocytes (eg, *Prdm16*, *Eps8l2*, *Pygl*, *Atp2a3*). Heatmaps generated from the *Chd4*^{AKO} snRNA-seq and bulk RNA-seq datasets (Figure 5F) confirmed that *Chd4* inactivation downregulated aCM-selective genes and upregulated skeletal and coronary artery tissue genes. Aggregate scores of genes specifically expressed in skeletal muscle myocytes (*Neb*, *Atp2a1*, *Kcnq5*, *Tnnt3*, *Tnnt1*) or smooth muscle myocytes (*Csrp1*, *Flna*, *Slit2*, *Myl9*, *Cald1*) compared with aCMs identified from the Genotype-Tissue Expression Project snRNA-seq atlas (Figure S5B and S5C) confirmed their upregulation in aCM_2 *Chd4*^{AKO} aCMs compared with control aCM_1 (Figure 5G). These data revealed that CHD4 is crucial for preventing misexpression of genes from other muscle lineages in postnatal aCMs.

A Dual Function for CHD4 in Enhancer Accessibility Maintenance and Repression

Next, we examined differences in chromatin accessibility between aCM_1 and aCM_2 (Figure 6A). There were 13 935 differentially accessible regions (DARs) between control and *Chd4*^{AKO} aCMs (aCM_1 versus aCM_2), with 2471 and 11 464 regions having greater accessibility in aCM_1 (control DARs) or aCM_2 (*Chd4*^{AKO} DARs) aCMs, respectively (Table S5). The greater number of regions with increased accessibility after *Chd4* inactivation is consistent with its canonical function as a repressor in the NuRD complex.[28] Most control DARs (83.6%; 2061 regions) were CHD4 bound, suggesting that CHD4 directly participates in maintaining the accessibility of these regions. In contrast, CHD4 bound only 41.5% (4760 regions) of *Chd4*^{AKO} DARs, suggesting that CHD4 governs the accessibility of these regions by a mix of direct and indirect mechanisms. To determine how region accessibility affected gene expression, we compared the transcript levels of genes near control and *Chd4*^{AKO} DARs in aCM_1 and aCM_2 (Figure 6B). Compared with genes neighboring regions that were not differentially accessible, genes near control DARs overall were expressed at greater levels in aCM_1, and genes near *Chd4*^{AKO} DARs were expressed at greater levels in aCM_2, consistent with control and *Chd4*^{AKO} DARs acting as enhancer or repressor cis-regulatory elements, respectively.

To determine whether control DARs act as aCM enhancers regulated by CHD4 and TBX5, we analyzed the active enhancer mark H3K27ac at control and *Chd4*^{AKO} DARs in *Tbx5*^{AKO} aCMs, *Chd4*^{AKO} aCMs, and respective control aCMs. Control DARs exhibited H3K27ac signal in WT aCMs, consistent with enhancer activity of these regions (Figure S6A). Either *Tbx5* or *Chd4* inactivation reduced both H3K27ac signal intensity and chromatin accessibility, indicating that both factors stimulate enhancer activity. Unlike control DARs, *Chd4*^{AKO} DARs had little detectable H3K27ac signal in WT aCMs (Figure S6B), consistent with *Chd4*^{AKO} DARs functioning as repressor rather than enhancer elements in control aCMs.

TBX5 enhanced CHD4 binding at 33 170 genomic loci and impaired CHD4 binding at 363 genomic loci (Figure 1C). Intersecting these regions with control and *Chd4*^{AKO} DARs revealed that TBX5 enhanced CHD4 binding at a greater proportion of control (1168 of 2471 [47.3%]) compared with *Chd4*^{AKO} (1302 of 14 464 [11.4%]) DARs (Figure 6C through 6E) while impairing CHD4 binding at only 4 (0.2%) control and 19 (0.1%) *Chd4*^{AKO} DARs, respectively (Figure 6D and 6E). Because

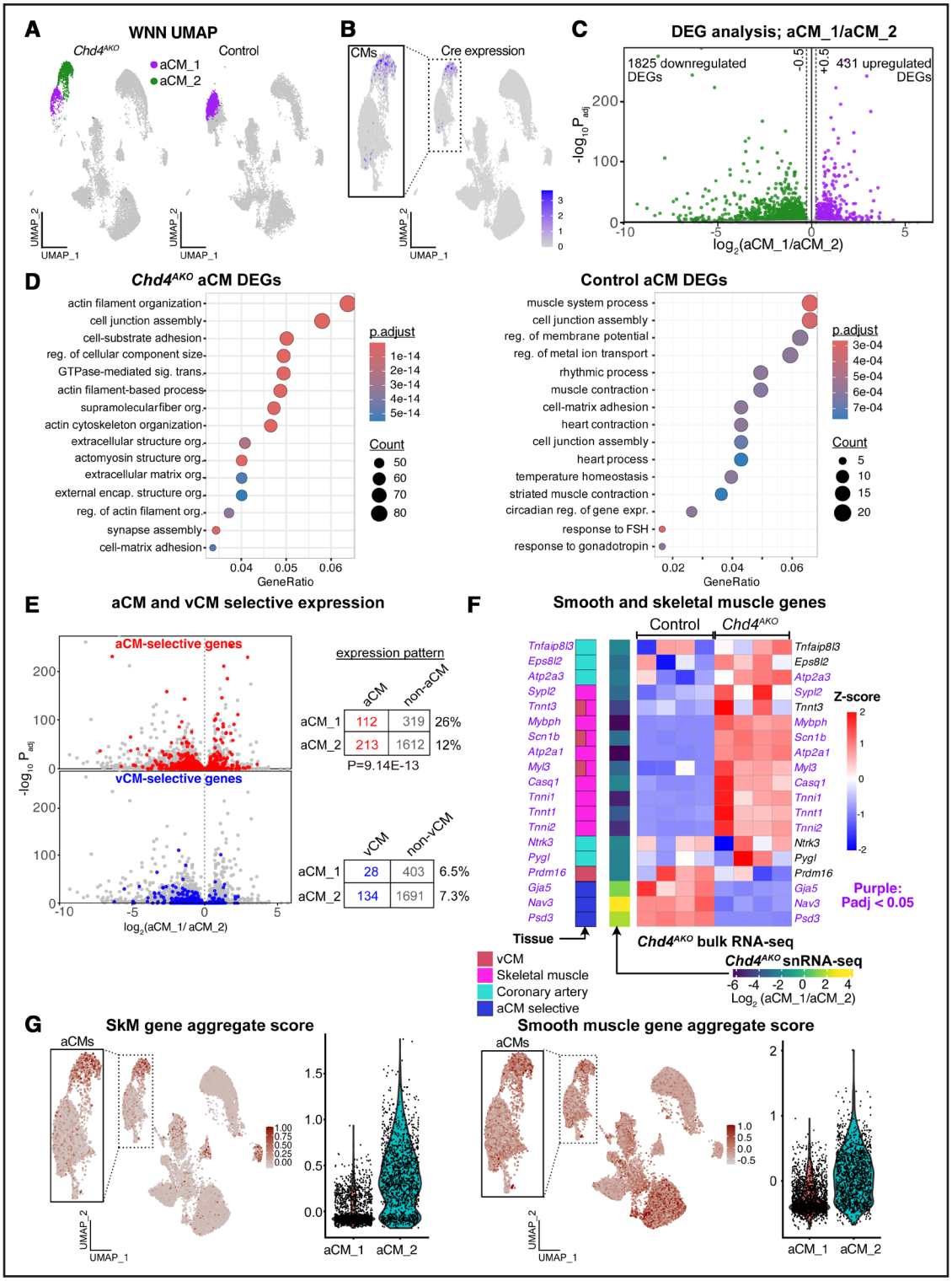

Figure 5. Combined snRNA-seq and snATAC-seq identifies distinct wild-type and CHD4AKO atrial cardiomyocyte cell states.
A, Concurrent single-nucleus RNA sequencing (snRNA-seq) and single-nucleus assay for transposase-accessible chromatin using sequencing (snATAC-seq) comparison of *Chd4*^{AKO} (n=4) and control (n=2) atria. Weighted nearest neighbor (WNN) uniform manifold and approximation projection (UMAP) integration of both data types is split by sample type. aCM_1 and aCM_2 predominantly originated from *Chd4*^{AKO} and control atria, respectively. **B**, The expression of *Cre* was projected onto the WNN UMAP. *Cre* is predominately detected in aCM_2. **C**, Pseudobulk RNA sequencing analysis of genes differentially expressed (|Log2FC|>0.5 and $P_{adjusted}$<0.05) between aCM_1 (control) and aCM_2 (*Chd4*^{AKO}). *P* values, Wilcoxon test with Benjamini-Hochberg (BH) correction. **D**, Gene Ontology terms enriched for differentially expressed genes (DEGs) more highly expressed in *Chd4*^{AKO} or control samples. *P* values, hypergeometric test with BH correction. **E**, Altered expression of atrial cardiomyocyte (aCM)– and ventricular cardiomyocyte (vCM)–selective genes in *Chd4*^{AKO} or control aCMs. Red and blue dots indicate aCM-selective and vCM-selective DEGs, respectively, as defined in Cao et al[1] (GSE215065). Contingency tables and the results of the Fisher test are shown (*Continued*)

Figure 5 Continued. to the right. **F**, Expression of smooth muscle and skeletal muscle genes in *Chd4*^{AKO} and control aCMs. The left-most column indicates normal tissue-selective expression based on the Genotype-Tissue Expression Project (Figure S5). The next column indicates fold change in gene expression from aCM_1 vs aCM_2. The main heatmap indicates row-scaled expression in bulk RNA sequencing from *Chd4*^{AKO} vs control atria. Genes colored purple were significantly differentially expressed in the snRNA-seq or bulk RNA sequencing experiments, respectively. **G**, Aggregate scores were determined using the expression of skeletal muscle genes *Neb*, *Atp2a1*, *Kcnq5*, *Tnnt3*, and *Tnnt1*, or smooth muscle genes *Csrp1*, *Flna*, *Slit2*, *Myl9*, and *Cald1*, and projected onto the UMAP. A violin plot was created showing the aggregate score in cells from aCM_1 and aCM_2.

TBX5 is required to activate aCM-selective genes in aCMs, we assessed the relationship of control and *Chd4*^{AKO} DARs to the regulation of aCM-selective genes. Control DARs neighbored 3-fold more aCM-selective genes than vCM-selective genes (15.7% versus 4.2%; Figure S6H), greater enrichment than observed for *Chd4*^{AKO} DARs (11.1% versus 6.2%; Figure S6H). These data suggest that CHD4 cooperates with TBX5 to activate aCM-selective genes in aCMs.

To further evaluate the effect of TBX5-enhanced control and *Chd4*^{AKO} DARs on the expression of aCM- and vCM-selective genes, we analyzed the association of these regions with aCM-, vCM-, or nonselective genes and the changes in gene expression caused by the inactivation of *Chd4* (Figure 6F and 6G). Of the 206 TBX5-enhanced control DARs neighboring aCM genes, 97 (47.1%) were associated with aCM-selective genes with greater expression in aCM_1 compared with aCM_2 (Figure 6F). Other functionally important genes without chamber-selective expression that were activated by TBX5-enhanced control DARs included *Ryr2* and *Rbm20*, both implicated in AF.[29–31] Together, these data underscore the importance of TBX5-enhanced CHD4 binding to activate aCM-selective genes and genes important for atrial rhythm homeostasis.

The parallel analysis of the 1302 TBX5-enhanced *Chd4*^{AKO} DARs revealed that 79 regions neighbored vCM-selective genes, 36 (45.5%) of which were repressed downstream of CHD4 (Figure 6G). Of the 162 TBX5-enhanced *Chd4*^{AKO} DARs associated with aCM-selective genes, 59 (36.4%) were repressed by CHD4. The repressed aCM-selective genes included *Atp2a1* and *Myl1*, which are expressed at greater levels in aCMs than vCMs but are more often associated with skeletal muscle, and *Tgfb2*, associated with chamber remodeling. These data indicate that TBX5-enhanced CHD4 binding and repression contributes to aCM gene regulation.

Together, these data reveal dual repressive and activating functions of CHD4 in aCMs. TBX5 recruits CHD4 to a set of genomic loci to activate a subset of aCM-selective genes. At the same time, TBX5 recruits CHD4 to distinct loci to repress gene expression, consistent with previous studies.[15]

CHD4 Enhances TBX5 Binding at Specific Loci

Given the loss of accessibility at control DARs (Figure 6A), we wondered whether CHD4 inactivation altered the binding of TFs to these regions. To test this hypothesis, we applied a recently reported deep learning framework, Seq2PRINT,[32] to pseudobulk snATAC data from aCM_1 and aCM_2 aCMs, as well as *Tbx5*^{AKO} and control aCMs, to predict TF binding. We initially used Seq-2PRINT to study the promoter and 2 putative enhancers of *Myl4* accessible regions bound by TBX5 (Figure S7A). The obtained footprints were <100 bp, as expected for TFs. CHD4 or TBX5 inactivation reduced the density of a subset of these footprints compared with control (arrows, Figure S7A, top). Predictive TF binding scores were high at the enhancer regions within the TBX5 ChIP summit. These scores were reduced in *Tbx5*^{AKO} (Figure S7A, middle and bottom), consistent with loss of TBX5 binding. The TF binding score was also lower in aCM_2, predicting that inactivation of *Chd4* reduced TBX5 binding.

To determine whether the predicted loss of TF binding was broadly applicable to regions that lose accessibility in *Chd4*^{AKO} aCMs, we calculated TF binding scores for TBX5, MEF2C, GATA4, and NKX2-5 at TBX5-enhanced control DARs (Figure S7B and S7C, quantified in Figure S7D). Binding scores of these 4 TFs were significantly lower in *Tbx5*^{AKO} aCMs (Figure S7C and S7D), consistent with their collaborative binding with TBX5.[1,24] Inactivation of *Chd4* reduced binding scores of TBX5 and MEF2C but not GATA4 or NKX2-5 (Figure S7B and S7D). This result predicts that CHD4 promotes TBX5 chromatin occupancy.

To test this prediction, we performed CUT&RUN for TBX5 in control and *Chd4*^{AKO} atria (Figure 7A). We used 2 primary antibodies recognizing TBX5 and performed each reaction in biological duplicate, producing 4 control samples and 4 *Chd4*^{AKO} samples. TBX5-bound regions identified by either antibody were enriched for similar motifs, including the TBX5 motif (Figure 7B). PCA analysis of binding intensities of the union of regions bound across all samples showed good agreement between antibodies. Furthermore, samples clustered by genotype, indicating that *Chd4* inactivation significantly altered TBX5 chromatin occupancy (Figure 7C).

We compared TBX5 occupancy in control or *Chd4*^{AKO} aCMs (Figure 7D). At control DARs, *Chd4* inactivation reduced TBX5 occupancy (Figure 7D, right), mirroring the effect of *Tbx5* inactivation on CHD4 occupancy (Figure 7D, left). In comparison to control DARs, binding differences at *Chd4*^{AKO} DARs were small. We used Diffbind[19] to better quantify differences in TBX5 binding between control and *Chd4*^{AKO} samples. At the

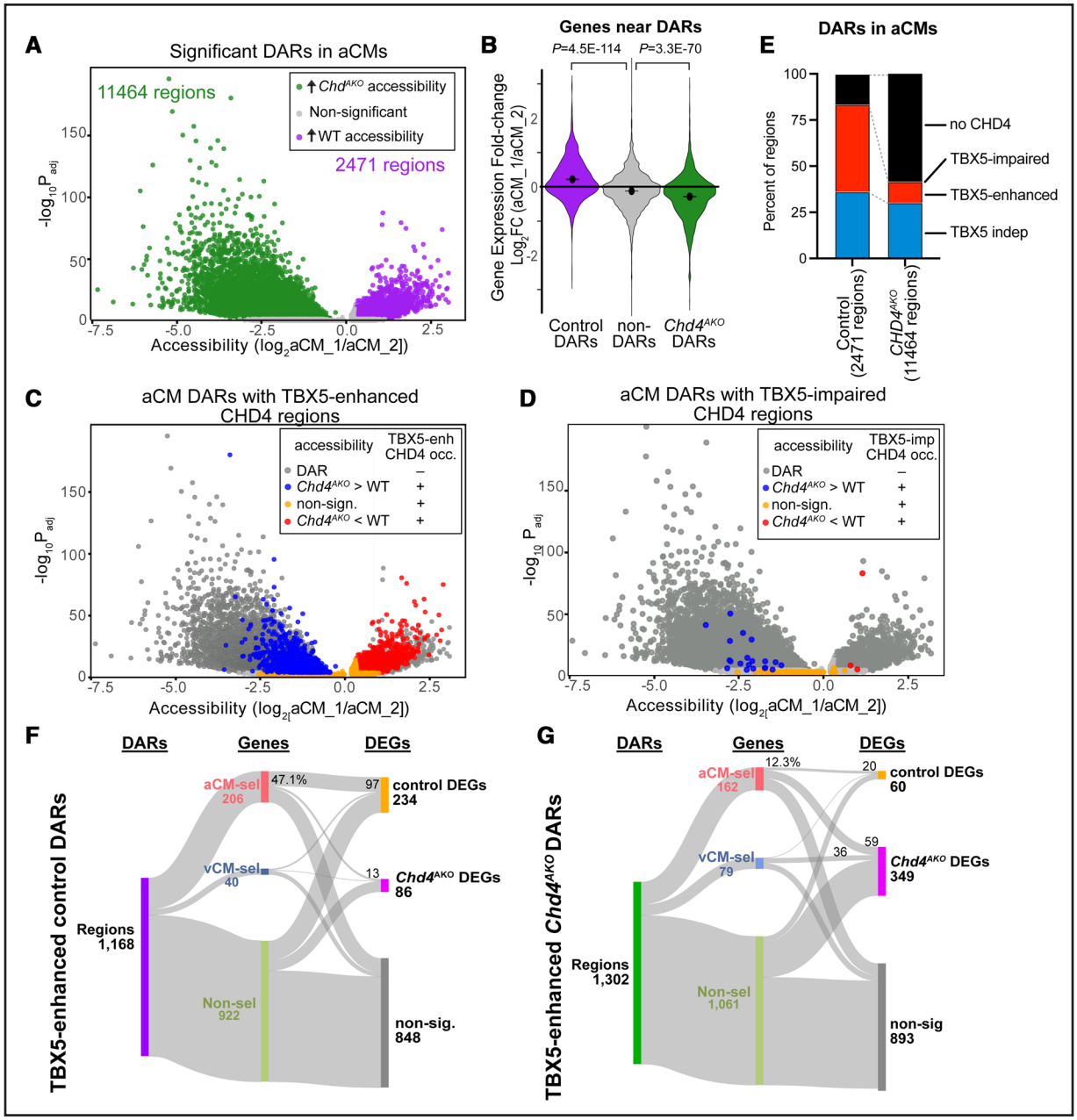

Figure 6. Transcriptional activation by TBX5-recruited CHD4.

A, Differentially accessible regions (DARs) in aCM_1 vs aCM_2. DARs were defined by $|Log_2FC|>0.25$ and $P_{adjusted}<0.05$. Adjusted *P* values, likelihood ratio test with Benjamini-Hochberg (BH) correction. **B**, The Log_2FC of gene expression in aCM_1/aCM_2 is plotted for genes near control DARs, *Chd4*^{AKO} DARs, or non-DAR regions. Wilcoxon rank-sum test. **C** and **D**, DARs colored by their overlap with TBX5 (T-box 5)–enhanced (**C**) and TBX5-impaired (**D**) CHD4 (chromodomain helicase DNA binding protein 4) regions. **E**, The proportion of control or *Chd4*^{AKO} DARs overlapping with TBX5-enhanced, TBX5-impaired, and TBX5-independent regions. **F** and **G**, Control or *Chd4*^{AKO} DARs with TBX5-enhanced CHD4 occupancy were classified as neighboring atrial cardiomyocyte (aCM)–selective, ventricular cardiomyocyte (vCM)–selective, or nonselective (not differentially expressed between aCMs and vCMs) genes. Regions were further classified by association with DEGs that were upregulated in aCM_1 (control), aCM_2 (*Chd4*^{AKO}), or neither. Numbers indicate number of regions.

union of peak regions across all the samples (61 935 regions; Figure 7E and 7F; Table S6), 10 154 regions had enhanced TBX5 binding in control aCMs compared with *Chd4*^{AKO} aCMs, and only 819 regions had increased TBX5 binding in *Chd4*^{AKO} aCMs. Of the 10 154 regions with CHD4-enhanced TBX5 binding, 4642 were bound by CHD4, and TBX5 enhanced CHD4 binding at 3051 of these regions (Figure 7E); ie, at these 3051 regions, TBX5 and CHD4 promoted each other's binding. The overlap between CHD4-enhanced TBX5 regions and TBX5-enhanced CHD4 regions was highly significant (Figure 7G).

We visualized these chromatin changes at the regulatory regions of 2 aCM-selective genes that are

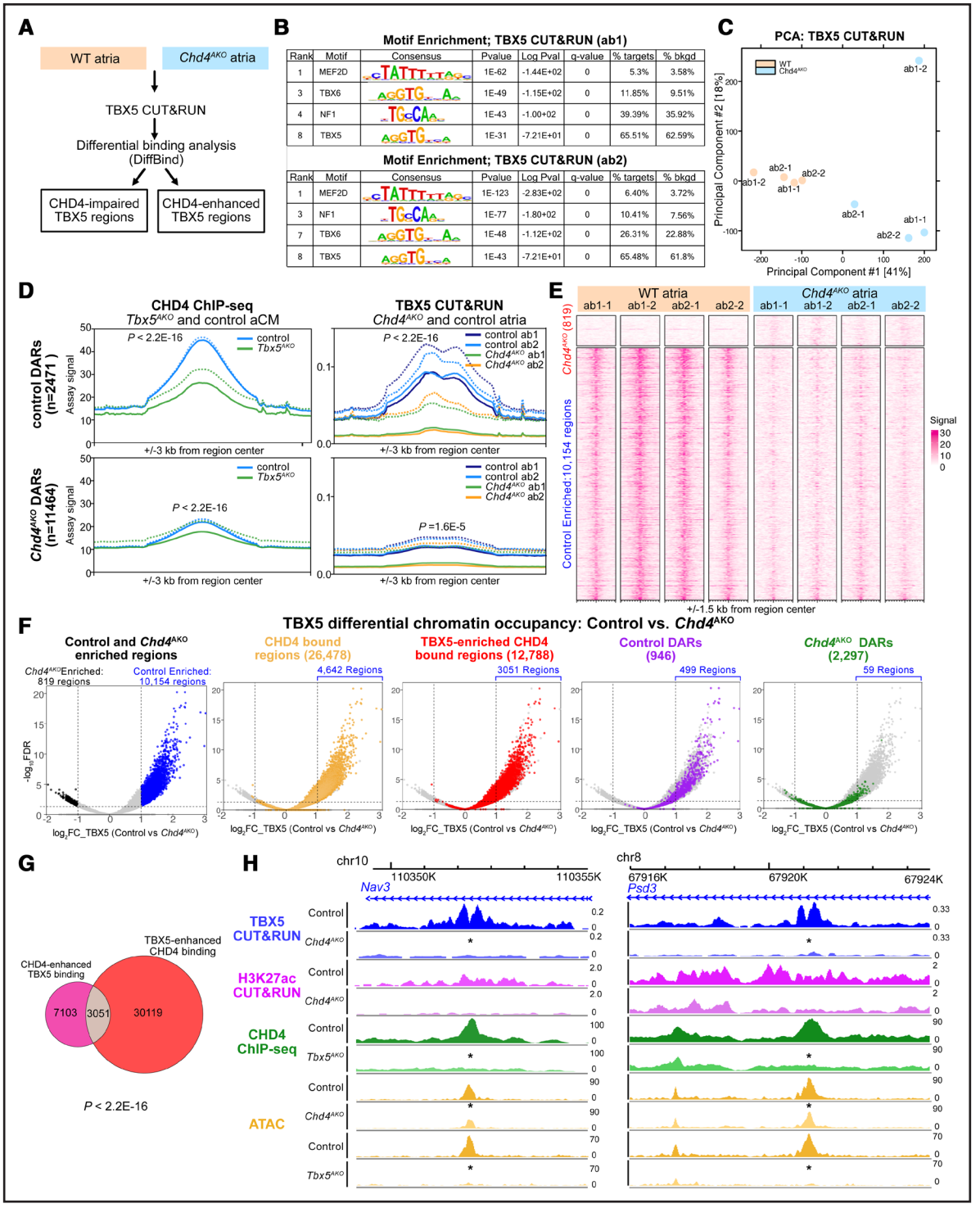

Figure 7. CHD4 promotes TBX5 genomic occupancy.

A, Experimental design of the TBX5 (T-box 5) cleavage under targets and release using nuclease (CUT&RUN). Atria were pooled from 5 postnatal day ≈21 (P21) control or *Chd4*^{AKO} mice per replicate. A total of 500 000 nuclei were used as an input for each reaction. Two antibodies were used in separate CUT&RUN pulldown experiments. Two biological replicates were performed for each antibody for each genotype, for a total of 4 control samples and 4 *Chd4*^{AKO} samples. **B**, Motif enrichment analysis was performed on peaks called from control samples for each antibody using HOMER. q values, hypergeometric test with Benjamini-Hochberg (BH) adjustment. **C**, Principal component analysis was performed using binding intensity of each sample across a unified peak set (all peaks called for each sample). Samples clustered by genotype, rather than by primary antibody used in the experiment. **D**, CHD4 (chromodomain helicase DNA binding protein 4) binding signal (from CHD4 atrial cardiomyocyte [aCM] chromatin immunoprecipitation followed by next-generation sequencing [ChIP-seq]) and TBX5 (T-box 5) binding signal (from TBX5 CUT&RUN) at control and *Chd4*^{AKO} differentially accessible regions (DARs). Wilcoxon rank sum test of signal intensity at the center 100 bp of the region. Solid and dotted lines indicate biological duplicate samples. **E** and **F**, Diffbind analysis comparing 4 control (*Continued*)

Figure 7 Continued. with 4 *Chd4*^{AKO} samples. **E**, Binding signal for each TBX5 replicate at regions with differential TBX5 binding affinity in control and *Chd4*^{AKO} samples, determined by DiffBind. **F**, TBX5 differential chromatin occupancy. Left, regions with greater TBX5 binding in control or *Chd4*^{AKO} ($|Log_2FC|>1$, false discovery rate [FDR]<0.05) are colored blue and black, respectively. Bottom 5 panels, volcano plots of differentially bound regions. Orange regions, regions co-bound by CHD4; red regions, regions with greater CHD4 binding in wild-type (WT) aCMs compared with *Tbx5*^{AKO} aCMs. Purple regions are control DARs, with greater accessibility in control (aCM_1) compared with *Chd4*^{AKO} (aCM_2) aCMs. Green regions are *Chd4*^{AKO} DARs, with greater genomic accessibility in *Chd4*^{AKO} aCMs (aCM_2) compared with control (aCM_1). FDR calculated with BH. **G**, The overlap between TBX5-enhanced CHD4 binding sites and CHD4-enhanced TBX5 binding sites. Hypergeometric test. **H**, Data from TBX5 CUT&RUN and H3K27ac CUT&RUN in control and *Chd4*^{AKO}, CHD4 ChIP-seq from control and *Tbx5*^{AKO} aCMs, and assay for transposase-accessible chromatin (ATAC) data from *Chd4*^{AKO} (aCM_2), *Tbx5*^{AKO} and control aCMs (aCM_1 and control TBX5 aCMs) from each multiomics experiment are visualized at intronic enhancer regions of aCM-selective genes *Nav3* and *Psd3*. Asterisks represent $P_{adjusted}<0.05$ in signal intensity for each experiment.

downregulated in *Chd4*^{AKO} and *Tbx5*^{AKO} aCMs: *Nav3*, which regulates heart development, contraction, and morphology in zebrafish,[33] and *Psd3*, which neighbors a variant linked to AF by a recent genome-wide association study[34] (Figure 7H). *Chd4* inactivation reduced TBX5 occupancy as well as H3K27ac at these regions. *Tbx5* inactivation reduced CHD4 occupancy of these regions. Either *Chd4* or *Tbx5* inactivation reduced accessibility of these regions in aCMs compared with control.

Together, these data indicate that CHD4 and TBX5 function together to bind regulatory regions in the aCM genome and promote the expression of aCM genes.

CHD4 Co-occupancy With Other Cardiac Transcription Factors

Other CHD4-interacting TFs have important roles in atrial gene regulation, including GATA4 and NKX2-5.[20] Using previously generated biotin-mediated ChIP-seq data,[1] we examined TBX5, GATA4, MEF2A, MEF2C, NKX2-5, SRF (serum response factor), and TEAD1 (TEA domain family member 1) occupancy at *Chd4*^{AKO} and control DARs in WT aCMs (Figure S8A). TBX5 was the most prominently bound TF at both control and *Chd4*^{AKO} DARs; TBX5 bound 53% of control DARs. NKX2-5 and GATA4, known CHD4 interactors, co-occupied 26.8% and 11.1% of control DARs, respectively, and TEAD1 co-bound 24.0% of control DARs. These data reveal TBX5 as the primary factor that recruits CHD4 as an activator, with other TFs playing lesser roles. A smaller percentage of *Chd4*^{AKO} DARs were bound by TBX5 (19%) or other cardiac TFs, suggesting that CHD4 recruitment to repressed loci predominantly occurs through mechanisms independent of binding to these major cardiac TFs.

To identify other TFs that participate in CHD4 recruitment, we performed motif enrichment analysis on CHD4-occupied control and *Chd4*^{AKO} DARs (Figure S8B; full list in Table S7). Many motifs (91) were enriched in both control and *Chd4*^{AKO} DARs, including motifs for TBX5, MEF2A/C, and GATA2/4/6. Among the 30 motifs uniquely enriched in control DARs, the top ranked motif belonged to the glucocorticoid receptor, implicated in cardiac fibrosis by interactions with the mineralocorticoid receptor (NR3C2), another control-enriched motif.[35] Among the 147 motifs enriched in *Chd4*^{AKO} DARs, top uniquely enriched motifs belonged to Fos and AP-1, transcriptional regulators of immediate early stress responses, and ETS family transcriptional regulators, implicated in atrial remodeling and arrhythmia.[36]

CHD4 Regulates AF-Associated Genes

TBX5-enhanced CHD4 binding activates and represses hundreds of genes in aCMs, including genes selectively expressed in aCMs, and the AF phenotype of *Chd4*^{AKO} mice demonstrates that these genes support atrial rhythm maintenance. Thus, we compared genes that are upregulated or downregulated in aCMs by inactivation of CHD4 or TBX5 with 241 genes associated with human AF by GWAS or familial studies[4] (Figure S9A). A total of 42 human AF genes were regulated by both CHD4 and TBX5, including *MYL4*, which was enhanced by CHD4 and TBX5 (Figure S9B).

The *Myl4* locus contains 2 predicted enhancers with TBX5 and CHD4 occupancy, chromatin accessibility, and flanking H3K27ac signal (blue highlights, Figure S9C). H3K27ac HiChIP from aCMs[9] revealed that *Myl4*_enh2 contacts the *Myl4* promoter and *Myl4*_enh1 adjoined a loop anchor also contacting the promoter. Correlation between the accessibility of these regions and *Myl4* expression further supported the function of these regions as *Myl4* enhancers (Signac linkage, Figure S9C). *Tbx5* inactivation reduced CHD4 occupancy, chromatin accessibility, and flanking H3K27ac signal at *Myl4*_enh1, *Myl4*_enh2, and the *Myl4* promoter (green highlight, Figure S9C). Inactivating CHD4 similarly reduced TBX5 occupancy, flanking H3K27ac, and genomic accessibility of the regions.

To further investigate CHD4 and TBX5 regulation of *Myl4*_enh1, we constructed a reporter AAV in which *Myl4*_enh1 and a minimal promoter drive atrial expression of GFP (Figure S9D). The vector also contains an RNA polymerase III promoter driving a noncoding *Broccoli* transcript, which serves as an internal control. The *Myl4*_enh1 reporter AAV was injected with (AKO) or without (control) AAV9:*Nppa-Cre* into *Chd4*$^{flox/flox}$ or *Tbx5*$^{flox/flox}$ mice, and enhancer activity was measured by the level of *GFP* transcript normalized to *Broccoli*. Inactivation of either *Chd4* or *Tbx5* significantly reduced *Myl4*_enh1

enhancer activity (Figure S9E). These data indicate that TBX5 and CHD4 coordinately stimulate *Myl4*_enh1 and *Myl4*_enh2 to activate *Myl4* transcription.

Together these results support TBX5 and CHD4 regulation of multiple genes implicated in human AF.

DISCUSSION

This study established that CHD4 is essential to maintain aCM function and atrial rhythm homeostasis. We showed that CHD4 has dual activities in aCM gene regulation. First, consistent with previous studies,[16,20] we confirmed that CHD4 transcriptionally represses genes not normally expressed in cardiomyocytes, such as those characteristic of skeletal and smooth muscle (Figure 8, CHD4 repressor role). Second, we revealed that CHD4 transcriptionally activates genes, including several selectively expressed in aCMs (Figure 8, CHD4 activator role).

CHD4 was required to repress sarcomeric genes of noncardiac muscle lineages, consistent with previous reports.[16,20] CHD4 canonically represses genes as a component of the NuRD complex, although some CHD4 functions are reported to be independent of the NuRD complex.[37] TBX5-dependent CHD4 recruitment accounted for a small fraction of genes repressed by CHD4 in aCMs; only 11.4% of regions that gained accessibility in *Chd4*^{AKO} aCMs had TBX5-dependent CHD4 occupancy. Other cardiac TFs likewise co-occupied a minority of *Chd4*^{AKO} DARs. These data demonstrate that CHD4's previously described function of repressing noncardiomyocyte sarcomere genes[15,16] in fetal and ventricular cardiomyocytes is active in adult aCMs.

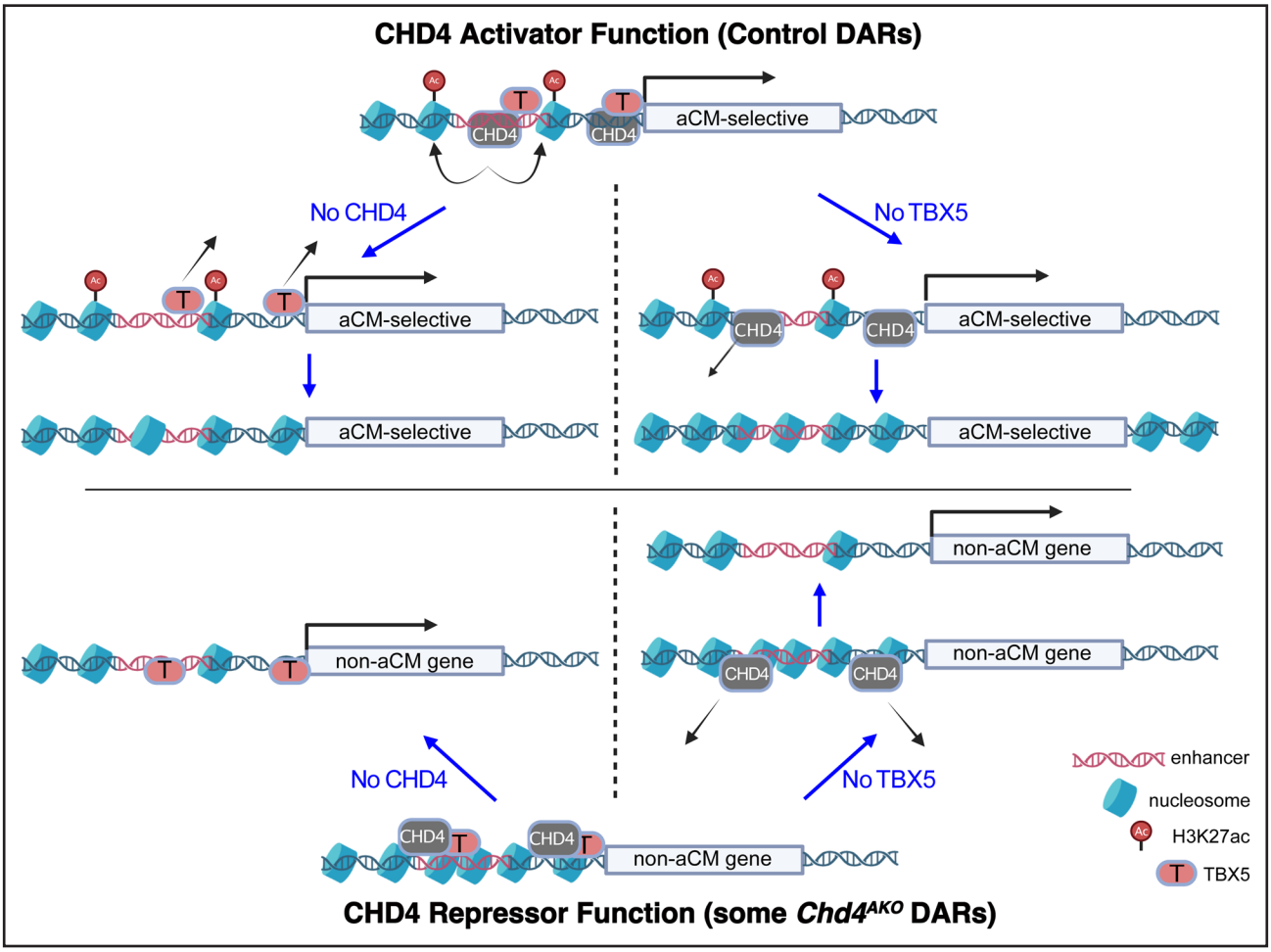

Figure 8. Model of TBX5-associated CHD4 activator and repressor functions.
Top, CHD4 (chromodomain helicase DNA binding protein 4) activator function. TBX5 (T-box 5) recruits CHD4 to enhancer elements and promoters to maintain their accessibility. Inactivating CHD4 results in the loss of CHD4 and TBX5 from these regions, and the loss of genomic accessibility, leading to enhancer inactivation and gene downregulation. Inactivating TBX5 similarly results in the loss of CHD4 because TBX5 is necessary to recruit CHD4 to these regions. Enhancers similarly close and the gene is downregulated. **Bottom**, CHD4 repressor function. TBX5 recruits CHD4 to limit enhancer accessibility. The loss of CHD4 results in increased accessibility and gene activation. The loss of TBX5 reduces CHD4 recruitment, similarly causing increased accessibility and gene activation. No significant loss of TBX5 to *Chd4*^{AKO} differentially accessible regions (DARs) was observed in the *Chd4*^{AKO}. aCM indicates atrial cardiomyocyte.

We found that CHD4 has a novel transcriptional activator function in aCMs tied to its requirement to maintain accessibility at 2471 loci. This CHD4 activating function was closely aligned with TBX5, as TBX5 enhanced CHD4 occupancy at 47% of these control DARs. These data support a model in which TBX5 recruits CHD4 through their previously described physical interaction,[14] increasing chromatin accessibility and activating gene transcription. CHD4-mediated recruitment of TBX5 and other TFs is a second mechanism by which CHD4 may activate gene transcription. CHD4 promoted TBX5 chromatin occupancy at 10 154 regions. Indeed, CHD4 and TBX5 reinforced each other's binding at 3051 regions.

Our results establish CHD4 as the first chromatin remodeling enzyme associated with AF and a key epigenetic regulator required for atrial homeostasis. Ablation of *Tbx5* in postnatal aCMs caused rapid development of spontaneous AF because of loss of aCM identity[9] and misexpression of $Ca2^{+}$ handling genes.[10,11] Here we show that CHD4 cooperates with TBX5 to maintain aCM enhancer accessibility and activate the expression of aCM-selective genes. Of 241 genes associated with increased AF risk by human genetics,[38–40] 95 are regulated by TBX5 (n=26), CHD4 (n=27), or both (n=42). Although these studies have not implicated CHD4 and other NuRD complex members in human AF, they have implicated cardiac TFs that bind CHD4 (TBX5, GATA4, and NKX2-5).[34,41] Of the AF risk genes coregulated by CHD4 and TBX5, 9 (*Tbx5*, *Mtss1*, *Myl4*, *Kcnq1*, *Nppa*, *Dpf3*, *Gja1*, *Myo18b*, and *Casz1*) had the hallmarks of being stimulated by the TBX5-dependent CHD4 gene activation mechanism: co-occupied by TBX5-enhanced CHD4 binding, loss of accessibility with *Chd4* inactivation, and downregulation with inactivation of either *Tbx5* or *Chd4*. That TBX5–CHD4 activates *Tbx5* itself suggests an intriguing feed-forward loop that reinforces aCM identity.

Patients initially develop paroxysmal AF and progress to sustained AF.[42] The mechanism by which episodes of AF remodel the atria's electrical properties to facilitate and sustain AF are unclear, but likely involves epigenetic alterations to the atrial gene program. *CHD4* is well positioned to be a central epigenetic factor that participates in the transcriptional reprogramming that accompanies AF progression. Additional studies are needed to test this intriguing hypothesis.

Limitations

Our study shows that TBX5 and CHD4 coordinately promote the accessibility of control DARs and activate aCM gene expression, but additional studies are required to elucidate the mechanisms by which CHD4 and TBX5 directly and indirectly cooperate to promote aCM gene transcription. Although the data are consistent with CHD4 and TBX5 functioning as components of a molecular complex that promotes gene transcription, we cannot exclude alternative models in which TBX5 and CHD4 act sequentially. Another important question is whether CHD4 activates transcription as a component of the NuRD complex, which canonically represses transcription,[43] or as a component of a novel regulatory complex. TBX5 was the predominant cardiac TF bound at control DARs occupied by CHD4, but CHD4 binds other cardiac TFs, including GATA4 and NKX2-5,[20] and it will be important to determine whether CHD4 can likewise partner with these other TFs to activate transcription.

ARTICLE INFORMATION

Received January 11, 2025; accepted July 2, 2025.

Affiliations

Department of Cardiology, Boston Children's Hospital, MA (M.E.S., Y.Y.S., Jie Li, Jiajin Li, E.M.K., A.P., Q.M., C.P., M.A.T., Y.W., C.H., V.J.B., W.T.P.). Department of Biology, University of North Carolina at Chapel Hill (W.S., F.L.C.). Division of Cardiology, Department of Internal Medicine, University of Nebraska Medical Center, Omaha (W.S.). Affiliated Hospital of Nanjing University of Chinese Medicine, Nanjing, China (Jie Li). Department of Cardiology, Children's Hospital of Chongqing Medical University, Chongqing, China (Jiajin Li). Department of Cardiology, Shanghai Children's Hospital, School of Medicine, Shanghai Jiao Tong University, China (C.H.). Harvard Stem Cell Institute, Cambridge, MA (W.T.P.).

Sources of Funding

This work was supported by grant K99HL173573 (Dr M.E. Sweat), the Center for Heart and Vascular Research COBRE (grant P20GM152326; Dr Shi), and grant R01HL156503 (Dr Pu).

Disclosures

None.

Supplemental Material

Methods
ARRIVE checklist
Figures S1–S9
Tables S1–S10
References 44–55

REFERENCES

1. Cao Y, Zhang X, Akerberg BN, Yuan H, Sakamoto T, Xiao F, VanDusen NJ, Zhou P, Sweat ME, Wang Y, et al. In vivo dissection of chamber-selective enhancers reveals estrogen-related receptor as a regulator of ventricular cardiomyocyte identity. *Circulation*. 2023;147:881–896. doi: 10.1161/CIRCULATIONAHA.122.061955
2. Wang Y, Wang J, Shi L, Chen X, Li D, Cui C, Yang K, Lu M, Huang J, Zhang L, et al. CIB2 is a novel endogenous repressor of atrial remodeling. *Circulation*. 2023;147:1758–1776. doi: 10.1161/CIRCULATIONAHA.122.062660
3. Zhou P, VanDusen NJ, Zhang Y, Cao Y, Sethi I, Hu R, Zhang S, Wang G, Ye L, Mazumdar N, et al. Dynamic changes in P300 enhancers and enhancer-promoter contacts control mouse cardiomyocyte maturation. *Dev Cell*. 2023;58:898–914.e7. doi: 10.1016/j.devcel.2023.03.020
4. Sweat ME, Pu WT. Genetic and molecular underpinnings of atrial fibrillation. *npj Cardiovascular Health*. 2024;1:e1–e35. doi: 10.1038/s44325-024-00035-5
5. Joglar JA, Chung MK, Armbruster AL, Benjamin EJ, Chyou JY, Cronin EM, Deswal A, Eckhardt LL, Goldberger ZD, Gopinathannair R, et al; Peer Review Committee Members. 2023 ACC/AHA/ACCP/HRS guideline for the diagnosis and management of atrial fibrillation: a report of the American College of Cardiology/American Heart Association joint committee on clinical practice guidelines. *Circulation*. 2024;149:e1–e156. doi: 10.1161/CIR.0000000000001193
6. Kathiriya IS, Dominguez MH, Rao KS, Muncie-Vasic JM, Devine WP, Hu KM, Hota SK, Garay BI, Quintero D, Goyal P, et al. A disrupted

compartment boundary underlies abnormal cardiac patterning and congenital heart defects. *bioRxiv*. Preprint posted online March 4th, 2024. doi: 10.1101/2024.02.05.578995
7. Bruneau BG, Logan M, Davis N, Levi T, Tabin CJ, Seidman JG, Seidman CE. Chamber-specific cardiac expression of Tbx5 and heart defects in Holt-Oram syndrome. *Dev Biol*. 1999;211:100–108. doi: 10.1006/dbio.1999.9298
8. Moskowitz IPG, Pizard A, Patel VV, Bruneau BG, Kim JB, Kupershmidt S, Roden D, Berul CI, Seidman CE, Seidman JG. The T-Box transcription factor Tbx5 is required for the patterning and maturation of the murine cardiac conduction system. *Development*. 2004;131:4107–4116. doi: 10.1242/dev.01265
9. Sweat ME, Cao Y, Zhang X, Burnicka-Turek O, Perez-Cervantes C, Arulsamy K, Lu F, Keating EM, Akerberg BN, Ma Q, et al. Tbx5 maintains atrial identity in post-natal cardiomyocytes by regulating an atrial-specific enhancer network. *Nat Cardiovasc Res*. 2023;2:881–898. doi: 10.1038/s44161-023-00334-7
10. Dai W, Laforest B, Tyan L, Shen KM, Nadadur RD, Alvarado FJ, Mazurek SR, Lazarevic S, Gadek M, Wang Y, et al. A calcium transport mechanism for atrial fibrillation in Tbx5-mutant mice. *Elife*. 2019;8:e41814. doi: 10.7554/elife.41814
11. Nadadur RD, Broman MT, Boukens B, Mazurek SR, Yang X, van den Boogaard M, Bekeny J, Gadek M, Ward T, Zhang M, et al. Pitx2 modulates a Tbx5-dependent gene regulatory network to maintain atrial rhythm. *Sci Transl Med*. 2016;8:354ra115. doi: 10.1126/scitranslmed.aaf4891
12. Lickert H, Takeuchi JK, Von Both I, Walls JR, McAuliffe F, Adamson SL, Henkelman RM, Wrana JL, Rossant J, Bruneau BG. Baf60c is essential for function of BAF chromatin remodelling complexes in heart development. *Nature*. 2004;432:107–112. doi: 10.1038/nature03071
13. Takeuchi JK, Lou X, Alexander JM, Sugizaki H, Delgado-Olguín P, Holloway AK, Mori AD, Wylie JN, Munson C, Zhu Y, et al. Chromatin remodelling complex dosage modulates transcription factor function in heart development. *Nat Commun*. 2011;2:187. doi: 10.1038/ncomms1187
14. Waldron L, Steimle JD, Greco TM, Gomez NC, Dorr KM, Kweon J, Temple B, Yang XH, Wilczewski CM, Davis IJ, et al. The cardiac TBX5 Interactome Reveals a chromatin remodeling network essential for cardiac septation. *Dev Cell*. 2016;36:262–275. doi: 10.1016/j.devcel.2016.01.009
15. Wilczewski CM, Hepperla AJ, Shimbo T, Wasson L, Robbe ZL, Davis IJ, Wade PA, Conlon FL. CHD4 and the NuRD complex directly control cardiac sarcomere formation. *Proc Natl Acad Sci U S A*. 2018;115:6727–6732. doi: 10.1073/pnas.1722219115
16. Gómez-Del Arco P, Perdiguero E, Yunes-Leites PS, Acín-Pérez R, Zeini M, Garcia-Gomez A, Sreenivasan K, Jiménez-Alcázar M, Segalés J, López-Maderuelo D, et al. The chromatin remodeling complex Chd4/NuRD controls striated muscle identity and metabolic homeostasis. *Cell Metab*. 2016;23:881–892. doi: 10.1016/j.cmet.2016.04.008
17. Sumi-Ichinose C, Ichinose H, Metzger D, Chambon P. SNF2beta-BRG1 is essential for the viability of F9 murine embryonal carcinoma cells. *Mol Cell Biol*. 1997;17:5976–5986. doi: 10.1128/MCB.17.10.5976
18. Hulsurkar MM, Lahiri SK, Moore O, Moreira LM, Abu-Taha I, Kamler M, Dobrev D, Nattel S, Reilly S, Wehrens XHT. Atrial-specific LKB1 knockdown represents a novel mouse model of atrial cardiomyopathy with spontaneous atrial fibrillation. *Circulation*. 2021;144:909–912. doi: 10.1161/CIRCULATIONAHA.121.055373
19. Stark R, Brown G. DiffBind: differential binding analysis of ChIP-Seq peak data. Compiled April 15, 2025. http://bioconductor.org/packages/release/bioc/vignettes/DiffBind/inst/doc/DiffBind.pdf
20. Robbe ZL, Shi W, Wasson LK, Scialdone AP, Wilczewski CM, Sheng X, Hepperla AJ, Akerberg BN, Pu WT, Cristea IM, et al. CHD4 is recruited by GATA4 and NKX2-5 to repress noncardiac gene programs in the developing heart. *Genes Dev*. 2022;36:468–482. doi: 10.1101/gad.349154.121
21. Bruneau BG, Nemer G, Schmitt JP, Charron F, Robitaille L, Caron S, Conner DA, Gessler M, Nemer M, Seidman CE, et al. A murine model of Holt-Oram syndrome defines roles of the T-box transcription factor Tbx5 in cardiogenesis and disease. *Cell*. 2001;106:709–721. doi: 10.1016/s0092-8674(01)00493-7
22. Misra C, Chang S-W, Basu M, Huang N, Garg V. Disruption of myocardial Gata4 and Tbx5 results in defects in cardiomyocyte proliferation and atrioventricular septation. *Hum Mol Genet*. 2014;23:5025–5035. doi: 10.1093/hmg/ddu215
23. Ghosh TK, Song FF, Packham EA, Buxton S, Robinson TE, Ronksley J, Self T, Bonser AJ, Brook JD. Physical interaction between TBX5 and MEF2C is required for early heart development. *Mol Cell Biol*. 2009;29:2205–2218. doi: 10.1128/MCB.01923-08
24. Akerberg BN, Gu F, VanDusen NJ, Zhang X, Dong R, Li K, Zhang B, Zhou B, Sethi I, Ma Q, et al. A reference map of murine cardiac transcription factor chromatin occupancy identifies dynamic and conserved enhancers. *Nat Commun*. 2019;10:4907. doi: 10.1038/s41467-019-12812-3
25. He A, Kong SW, Ma Q, Pu WT. Co-occupancy by multiple cardiac transcription factors identifies transcriptional enhancers active in heart. *Proc Natl Acad Sci U S A*. 2011;108:5632–5637. doi: 10.1073/pnas.1016959108
26. Shi W, Wasson LK, Dorr KM, Robbe ZL, Wilczewski CM, Hepperla AJ, Davis IJ, Seidman CE, Seidman JG, Conlon FL. CHD4 and SMYD1 repress common transcriptional programs in the developing heart. *Development*. 2024;151:dev202505. doi: 10.1242/dev.202505
27. Hulsmans M, Schloss MJ, Lee I-H, Bapat A, Iwamoto Y, Vinegoni C, Paccalet A, Yamazoe M, Grune J, Pabel S, et al. Recruited macrophages elicit atrial fibrillation. *Science*. 2023;381:231–239. doi: 10.1126/science.abq3061
28. Lai AY, Wade PA. Cancer biology and NuRD: a multifaceted chromatin remodelling complex. *Nat Rev Cancer*. 2011;11:588–596. doi: 10.1038/nrc3091
29. Vad OB, Angeli E, Liss M, Ahlberg G, Andreasen L, Christophersen IE, Hansen CC, Møller S, Hellsten Y, Haunsoe S, et al. Loss of cardiac splicing regulator RBM20 is associated with early-onset atrial fibrillation. *JACC Basic Transl Sci*. 2024;9:163–180. doi: 10.1016/j.jacbts.2023.08.008
30. Laforest B, Dai W, Tyan L, Lazarevic S, Shen KM, Gadek M, Broman MT, Weber CR, Moskowitz IP. Atrial fibrillation risk loci interact to modulate Ca2+-dependent atrial rhythm homeostasis. *J Clin Invest*. 2019;129:4937–4950. doi: 10.1172/JCI124231
31. Gillis AM, Dobrev D. Targeting the RyR2 to prevent atrial fibrillation. *Circ Arrhythm Electrophysiol*. 2022;15:e011514. doi: 10.1161/CIRCEP.122.011514
32. Hu Y, Horlbeck MA, Zhang R, Ma S, Shrestha R, Kartha VK, Duarte FM, Hock C, Savage RE, Labade A, et al. Multiscale footprints reveal the organization of cis-regulatory elements. *Nature*. 2025;638:779–786. doi: 10.1038/s41586-024-08443-4
33. Lv F, Ge X, Qian P, Lu X, Liu D, Chen C. Neuron navigator 3 (NAV3) is required for heart development in zebrafish. *Fish Physiol Biochem*. 2022;48:173–183. doi: 10.1007/s10695-022-01049-5
34. Roselli C, Surakka I, Olesen MS, Sveinbjornsson G, Marston NA, Choi SH, Holm H, Chaffin M, Gudbjartsson D, Hill MC, et al; BioBank Japan Project. Meta-analysis of genome-wide associations and polygenic risk prediction for atrial fibrillation in more than 180,000 cases. *Nat Genet*. 2025;57:539–547. doi: 10.1038/s41588-024-02072-3
35. Yi Y, Du L, Qin M, Chen X-Q, Sun X-N, Li C, Du L-J, Liu Y, Liu Y, Sun J-Y, et al. Regulation of atrial fibrosis by the bone. *Hypertension*. 2019;73:379–389. doi: 10.1161/HYPERTENSIONAHA.118.11544
36. Rommel C, Rösner S, Lother A, Barg M, Schwaderer M, Gilsbach R, Bömicke T, Schnick T, Mayer S, Doll S, et al. The transcription factor ETV1 induces atrial remodeling and arrhythmia. *Circ Res*. 2018;123:550–563. doi: 10.1161/CIRCRESAHA.118.313036
37. O'Shaughnessy A, Hendrich B. CHD4 in the DNA-damage response and cell cycle progression: not so NuRDy now. *Biochem Soc Trans*. 2013;41:777–782. doi: 10.1042/BST20130027
38. Roselli C, Chaffin MD, Weng L-C, Aeschbacher S, Ahlberg G, Albert CM, Almgren P, Alonso A, Anderson CD, Aragam KG, et al. Multi-ethnic genome-wide association study for atrial fibrillation. *Nat Genet*. 2018;50:1225–1233. doi: 10.1038/s41588-018-0133-9
39. Nielsen JB, Thorolfsdottir RB, Fritsche LG, Zhou W, Skov MW, Graham SE, Herron TJ, McCarthy S, Schmidt EM, Sveinbjornsson G, et al. Biobank-driven genomic discovery yields new insight into atrial fibrillation biology. *Nat Genet*. 2018;50:1234–1239. doi: 10.1038/s41588-018-0171-3
40. Miyazawa K, Ito K, Ito M, Zou Z, Kubota M, Nomura S, Matsunaga H, Koyama S, Ieki H, Akiyama M, et al; BioBank Japan Project. Cross-ancestry genome-wide analysis of atrial fibrillation unveils disease biology and enables cardioembolic risk prediction. *Nat Genet*. 2023;55:187–197. doi: 10.1038/s41588-022-01284-9
41. Choi SH, Jurgens SJ, Xiao L, Hill MC, Haggerty CM, Sveinbjörnsson G, Morrill VN, Marston NA, Weng L-C, Pirruccello JP, et al; Regeneron Genetics Center. Sequencing in over 50,000 cases identifies coding and structural variation underlying atrial fibrillation risk. *Nat Genet*. 2025;57:548–562. doi: 10.1038/s41588-025-02074-9
42. Blum S, Aeschbacher S, Meyre P, Zwimpfer L, Reichlin T, Beer JH, Ammann P, Auricchio A, Kobza R, Erne P, et al; Swiss-AF Investigators. Incidence and predictors of atrial fibrillation progression. *J Am Heart Assoc*. 2019;8:e012554. doi: 10.1161/JAHA.119.012554
43. Basta J, Rauchman M. The nucleosome remodeling and deacetylase complex in development and disease. *Transl Res*. 2015;165:36–47. doi: 10.1016/j.trsl.2014.05.003

44. Williams CJ, Naito T, Arco PG-D, Seavitt JR, Cashman SM, De Souza B, Qi X, Keables P, Von Andrian UH, Georgopoulos K. The chromatin remodeler Mi-2beta is required for CD4 expression and T cell development. *Immunity*. 2004;20:719–733. doi: 10.1016/j.immuni.2004.05.005
45. Wang S, Guo Y, Pu WT. AAV gene transfer to the heart. *Methods Mol Biol*. 2021;2158:269–280. doi: 10.1007/978-1-0716-0668-1_20
46. Nadelmann ER, Gorham JM, Reichart D, Delaughter DM, Wakimoto H, Lindberg EL, Litviňukova M, Maatz H, Curran JJ, Ischiu Gutierrez D, et al. Isolation of nuclei from mammalian cells and tissues for single-nucleus molecular profiling. *Curr Protoc*. 2021;1:e132. doi: 10.1002/cpz1.132
47. Cui M, Olson EN. Protocol for single-nucleus transcriptomics of diploid and tetraploid cardiomyocytes in murine hearts. *STAR Protoc*. 2020;1:100049. doi: 10.1016/j.xpro.2020.100049
48. Yu G, Wang L-G, He Q-Y. ChIPseeker: an R/Bioconductor package for ChIP peak annotation, comparison and visualization. *Bioinformatics*. 2015;31:2382–2383. doi: 10.1093/bioinformatics/btv145
49. Cheshire C, West C, Rönkkö T, Bot N-C, Patel H, Hodgetts T, Ladd D, Thiery A, Fields C, Deu-Pons J, et al. nf-core/cutandrun: nf-core/cutandrun v3.2.2 Iridium Ibis. Zenodo. Published 2024. Accessed April 2, 2025. http://dx.doi.org/10.5281/zenodo.10606804
50. Meers MP, Tenenbaum D, Henikoff S. Peak calling by sparse enrichment analysis for CUT&RUN chromatin profiling. *Epigenetics Chromatin*. 2019;12:42. doi: 10.1186/s13072-019-0287-4
51. Stuart T, Srivastava A, Madad S, Lareau CA, Satija R. Single-cell chromatin state analysis with Signac. *Nat Methods*. 2021;18:1333–1341. doi: 10.1038/s41592-021-01282-5
52. Butler A, Hoffman P, Smibert P, Papalexi E, Satija R. Integrating single-cell transcriptomic data across different conditions, technologies, and species. *Nat Biotechnol*. 2018;36:411–420. doi: 10.1038/nbt.4096
53. McGinnis CS, Murrow LM, Gartner ZJ. DoubletFinder: doublet detection in single-cell RNA sequencing data using artificial nearest neighbors. *Cell Syst*. 2019;8:329–337.e4. doi: 10.1016/j.cels.2019.03.003
54. Ianevski A, Giri AK, Aittokallio T. Fully-automated and ultra-fast cell-type identification using specific marker combinations from single-cell transcriptomic data. *Nat Commun*. 2022;13:1246. doi: 10.1038/s41467-022-28803-w
55. Ma S, Zhang B, LaFave LM, Earl AS, Chiang Z, Hu Y, Ding J, Brack A, Kartha VK, Tay T, et al. Chromatin potential identified by shared single-cell profiling of RNA and chromatin. *Cell*. 2020;183:1103–1116.e20. doi: 10.1016/j.cell.2020.09.056